Tertiary Structure Stabilization Promotes Hairpin Ribozyme Ligation[†]

Martha J. Fedor*

Department of Molecular Biology and The Skaggs Institute for Chemical Biology, The Scripps Research Institute. 10550 North Torrey Pines Road, MB35, La Jolla, California 92037

Received May 11, 1999; Revised Manuscript Received June 23, 1999

ABSTRACT: The hairpin ribozyme catalyzes a reversible RNA cleavage reaction that participates in processing intermediates of viral satellite RNA replication in plants. A minimal hairpin ribozyme consists of two helix−loop−helix segments. These segments associate noncoaxially in the active folded structure in a way that brings catalytically important loop nucleotides into close proximity. The hairpin ribozyme in the satellite RNA of Tobacco Ringspot Virus assembles in the context of a four-way helical junction. Recent physical characterization of hairpin ribozyme structures using fluorescence resonance energy transfer demonstrated enhanced stability of the folded structure in the context of a four-way helical junction compared to minimal hairpin ribozyme variants. Analysis of the functional consequences of this modification of the helical junction has revealed two changes in the hairpin ribozyme kinetic mechanism. First, ribozymes with a four-way helical junction bind 3′ cleavage products with much higher affinity than minimal hairpin ribozymes, evidence that tertiary interactions within the folded structure contribute to product binding energy. Second, the balance between ligation and cleavage shifts in favor of ligation. The enhanced ligation activity of hairpin ribozymes that contain a four-way helical junction supports the notion that tertiary structure stability is a major determinant of the hairpin ribozyme proficiency as a ligase and illustrates the link between RNA structure and biological function.

The hairpin ribozyme belongs to the family of small catalytic RNAs that cleave RNA substrates in reactions that generate products with 5′-hydroxyl and 2′,3′-cyclic phosphate termini (reviewed in *1*). RNA-catalyzed ligation, a simple reversal of the cleavage reaction, joins these termini to form phosphodiesters (*2*). In contrast to the hammerhead ribozyme that favors cleavage over ligation by more than 100-fold (*3*, *4*), the hairpin ribozyme is a better ligase than it is a nuclease. Hairpin ribozyme rate constants for product ligation are ∼10-fold higher than rate constants for substrate cleavage when the ribozyme is saturated with cleavage products (*5*). In vivo, hairpin ribozyme sequences are found in satellite RNAs of plant viruses where ligation serves to generate circular templates for rolling circle replication (*6*−*8*).

A minimal hairpin ribozyme consists of two helix−loop−helix segments (*9*, Figure 1A). Most helical regions tolerate base pair substitutions without loss of activity while alterations of many loop nucleotides interfere with catalysis, evidence that unpaired nucleotides serve critical structural or catalytic roles. The solution structures of isolated loop A and loop B domains have been characterized by NMR (*10*, *11*), but no high-resolution structural data are yet available for the complete ribozyme. Results of mutagenesis, cross-linking, and chemical protection studies suggest that the two helix−loop−helix elements adopt a noncoaxial structure that brings loops A and B into close proximity (*12*−*17*, Figure 1A). The two loops have been proposed to interact through a "ribose zipper" motif (*18*) involving four 2′-hydroxyls (*15*). FRET[1] experiments recently have provided additional physical evidence of "docking" of the two helix−loop−helix segments in the folded tertiary structure and have identified specific structural features that influence the equilibrium between extended and folded states (*19*−*23*).

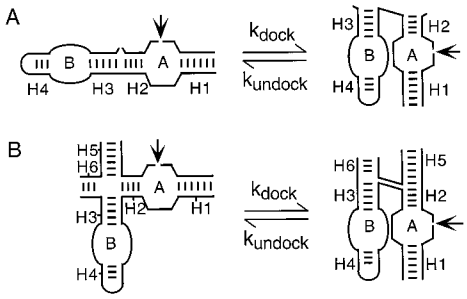

FIGURE 1: Models of hairpin ribozyme structures in extended and docked conformations. (A) A minimal hairpin ribozyme consists of four helical regions, H1 through H4, and two unpaired loops, A and B. The arrow marks the reactive phosphodiester in loop A. The two essential H1−loop A−H2 and H3−loop B−H4 elements associate noncoaxially within the folded tertiary structure. (B) The hairpin ribozyme sequence of (−)sTRSV includes two additional helices, H5 and H6, that create a four-way helical junction between the essential H1−loop A−H2 and H3−loop B−H4 elements. A tertiary structure model in which H3−H6 and H2−H5 form two pairs of coaxially stacked helices and loops A and B are in close proximity is consistent with distances between helix termini measured by FRET (*21*−*24*, *45*).

[†] This work was supported by NIH Grant RO1 GM46422.

* Address correspondence to this author. Phone: (858) 784-2770. FAX: (858) 784-2779 E mail: mfedor@scripps.edu.

[1] Abbreviations: (−)sTRSV, negative strand of the satellite RNA of Tobacco Ringspot Virus; FRET, fluorescence resonance energy transfer; R, ribozyme; LR, ligated ribozyme; 5′R, 5′ ribozyme; S, cleavage substrate; 3′P, 3′ cleavage product; HEPES, *N*-(2-hydroxyethyl)piperazine-*N*′-2-ethanesulfonic acid; EDTA, (ethylenedinitrilo)-tetraacetic acid; Tris, tris(hydroxymethyl)aminomethane; PCR, polymerase chain reaction.

10.1021/bi991069q CCC: $18.00
Published on Web 08/05/1999

In the natural context of Tobacco Ringspot Virus satellite RNA, the hairpin ribozyme is associated with two additional helices that are interposed between the two essential helix−loop−helix elements to create a four-way helical junction (*9*). FRET and comparative electrophoretic mobility studies support a model of the folded four-way helical junction that places the two essential helix−loop−helix elements in an antiparallel orientation with loops A and B juxtaposed (*21*, *24*, Figure 1B). The equilibrium distributions of extended and docked conformations of hairpin ribozymes with different junction structures have been compared through time-resolved FRET (*23*). These studies show that the active, docked conformation is more stable, by ~1 kcal/mol, in the context of a four-way helical junction relative to the docked conformation of a minimal ribozyme that contains only the essential helix−loop−helix segments.

The current work focuses on the functional consequences of the enhanced tertiary structure stability that is conferred by the natural four-way helical junction. Previously, hairpin ribozymes with a four-way helical junction were found to display reduced cleavage rates and low reaction extents relative to minimal hairpin ribozymes (*21*, *22*). Detailed analyses of cleavage and ligation reactions mediated by a hairpin ribozyme with a four-way helical junction show that an apparent drop in cleavage activity instead reflects two changes in the kinetic mechanism. First, ligation rate constants increase 6-fold. Enhanced ligation activity is consistent with our previous finding that reaction conditions that stabilize RNA structure tend to promote ligation more than cleavage (*25*). Second, ribozymes with a four-way helical junction bind 3′ cleavage products with ~50-fold higher affinity relative to minimal hairpin ribozyme sequences, under standard conditions including 10 mM $MgCl_2$ at 25 °C. An apparent loss of cleavage activity can be explained by a change in the partitioning of the ribozyme−product complex between ligation and product dissociation. In the context of a four-way helical junction, only 5% of all cleavage events are followed by product dissociation while ~95% are reversed by rapid re-ligation of bound product. These results point to the inextricable link between RNA structure and biological function.

EXPERIMENTAL PROCEDURES

Plasmid Templates for Transcription of 5′ Ribozyme RNAs. The plasmid pTLR26 that encodes a self-cleaving hairpin ribozyme variant with a two-way helical junction, LR26, was described previously (*25*). Sequences encoding H5 and H6 were inserted into pTLR26 to create pTLR46, the template for transcription of 5′R4. The insertion was accomplished through PCR amplification of the hairpin ribozyme cassette using the HPL3 primer described previously and a primer analogous to the HPL4 primer described previously but containing additional nucleotides that encode the H5 and H6 sequences and extending 15 nucleotides beyond the insertion. Plasmid sequences were confirmed by dideoxy sequencing using conventional procedures (*26*). Plasmids were propagated in *E. coli* strain DH5α.

Preparation of RNAs. Ribozyme, 5′ ribozyme, substrate, and 3′ product RNAs were prepared and labeled with ^{32}P as previously described (*5*, *25*, *27*, *28*, and references cited therein). Briefly, ribozyme RNAs used for intermolecular cleavage and ligation reactions were prepared through T7 RNA polymerase transcription of partially duplex synthetic oligonucleotide templates (*29*). [α-^{32}P]-labeled 5′ ribozyme RNA used for self-ligation reactions was prepared by T7 RNA polymerase transcription of *Bgl*II-linearized plasmid templates in reactions that included [α-^{32}P]ATP. To increase the yield of 5′ ribozyme that results from self-cleavage of the primary transcript, transcription reactions were incubated at 50 °C for 5 min before fractionation. The 5′ ribozyme fragment was then purified by denaturing gel electrophoresis. Cleavage substrates and 3′ cleavage product RNAs were synthesized chemically and deprotected as previously described (*5*) or were supplied by Dharmacon Research, Inc., and deprotected using the procedure recommended by the supplier. [5′-^{32}P]-labeled substrate RNAs were prepared by reaction with T4 polynucleotide kinase and [γ-^{32}P]ATP. All RNAs were gel-purified by denaturing gel electrophoresis and purified as sodium salts by DEAE-650M chromatography (Toyopearl). RNA concentrations were determined by assuming a residue extinction coefficient of 6.6×10^3 M^{-1} cm^{-1} at 260 nm or calculated from the specific activity of the [α-^{32}P]ATP used for labeling.

Kinetic and Equilibrium Analyses. Reactions were carried out at 25 °C in 50 mM NaHEPES, pH 7.5, 10 mM $MgCl_2$, 0.1 mM EDTA that was prepared using a standardized solution of 1 M $MgCl_2$ (Sigma) unless otherwise indicated. pH was adjusted appropriately for each reaction temperature. No significant change in kinetics or equilibrium parameters was detected in reactions carried out in NaHEPES buffers compared to reactions carried out in the Tris-HCl buffers used previously (*25*, *28*). Reaction components were combined immediately before use.

Rate constants and K_MS values were determined for intermolecular cleavage reactions in experiments with 0.1 nM [α-^{32}P]substrate and various concentrations of ribozyme in 10-fold or greater excess as described previously (*5*, *28*).

Self-cleavage rates were measured in pulse−chase experiments as described previously (*25*). Ligated ribozyme, LR24, was first prepared by combining 50 nM [α-^{32}P]5′R2 with 1 μM 3′P24 and incubating at 10 °C for ≥30 min. Ligated ribozyme, LR43, was prepared in a similar reaction with [α-^{32}P]-labeled 5′R4 and 0.3 μM 3′P3. Ligation reactions were then diluted 100- or 400-fold in reaction buffer equilibrated at the appropriate temperature, and the fraction of 5′R was measured after various times. Comparison of cleavage rates and extents in reactions with different dilution volumes confirmed that rapid dissociation and dilution of 3′P drove cleavage to completion after dilution. Samples were removed at intervals, quenched by 5-fold dilution into 8 M urea, 25 mM EDTA, 0.0002% bromophenol blue, 0.0002% xylene cyanole, and fractionated on denaturing gels. Bands corresponding to ligated ribozyme and 5′ ribozyme RNAs were quantitated by radioanalytic imaging (Molecular Dynamics). Cleavage rate constants were computed from fits to: fraction $5'R = e^{-k_{cleavage}t}$ after normalization to the fraction of ligated ribozyme at the start of the cleavage time course.

The sum of cleavage and ligation rate constants ($k_{ligation} + k_{cleavage}$) was measured as described previously (*25*). Briefly, 5 nM [α-^{32}P]-labeled 5′R2 or 5′R4 was combined with 5 or 25 μM 3′P8 in 50 mM NaHEPES, pH 7.5, 0.1 mM EDTA and allowed to equilibrate at 10 °C for ≥10 min to allow 5′R·3′P28 complex formation. Two microliters of

the RNA solution was then combined with 48 μL of reaction buffer at the appropriate temperature. Samples were removed at intervals, quenched, fractionated, and quantitated as described above. Observed ligation rates were determined by computing the fit to: fraction LR = $e^{k_{obs,\ ligation}t}$. Reactions with 5 or 25 μM 3′P8 gave the same observed ligation rates and the same fraction of ligated ribozyme at equilibrium, evidence that the concentration of 3′P8 was sufficiently high to saturate 5′ ribozyme complex formation during the initial binding reaction.

Ligation rate constants at temperatures from 15 to 25 °C were calculated from the difference between mean cleavage rate constants measured in pulse−chase experiments and the mean sum of cleavage and ligation rate constants measured in two or more ligation reactions. At temperatures below 15 °C, slow product dissociation interfered with direct measurement of self-cleavage rates. Therefore, ligation rate constants between 0 and 10 °C were calculated from the difference between the sum of cleavage and ligation rates measured directly in ligation reactions and cleavage rate constants that were extrapolated from cleavage rate constants that had been measured at higher temperatures based on the temperature dependence. Values used for thermodynamic calculations are the mean and range of self-cleavage and self-ligation rates obtained from two or more experiments. Errors calculated for thermodynamic parameters reflect the standard error derived from computed linear fits of Arrhenius and van't Hoff plots and an estimated error of 10% in cleavage rate constant measurements and of 20% in ligation rate constant measurements.

Apparent equilibrium dissociation constants for 5′R·3′P complexes were determined from the fraction of [α-^{32}P]5′R converted to [α-^{32}P]LR after ligation reactions with various excess concentrations of 3′P RNA were allowed to reach equilibrium, as described previously (*25*). The fraction of 5′R converted to LR by the end of a ligation reaction is the product of K_{eq}^{int}, that is, $k_{ligation}/k_{cleavage}$, and the fraction of 5′R bound by 3′P, or [3′P]/([3′P] + $K_d^{3'P}$). $K_{d,app}^{3'P}$ values were determined by computing the fit to fraction $LR_{t=\infty}$ = (LR_{sat})([5′R·3′P]/([5′R·3′P] + $K_{d,app}^{3'P}$) where $LR_{t=\infty}$ is the fraction of ligated ribozyme at equilibrium and LR_{sat} is the fraction of ligated ribozyme at equilibrium with a saturating concentration of 3′P.

Kinetic simulations were carried out using Kinetics Simulation 1.0 software (IBM Almaden Research Center, 1995).

RESULTS

Intermolecular Cleavage Kinetics. Intermolecular cleavage kinetics were examined for a hairpin ribozyme variant, R4, that contains a four-way helical junction (Figure 2). The sequence of R4 resembles that of a minimal hairpin ribozyme variant, R2, that we have characterized previously (*25*, *28*). The R2 and R4 sequences incorporate changes from the commonly studied (−)sTRSV-derived hairpin sequence that were designed to minimize incorrect folding and facilitate mechanistic studies (*5*, *25*, *30*). In the R4 sequence, a stem−loop structure that contains five base pairs and is capped by a stable tetraloop, H6, is inserted between the two essential helix−loop−helix domains. Additional 3′ terminal nucleotides allow a helix with four base pairs, H5, to form upon

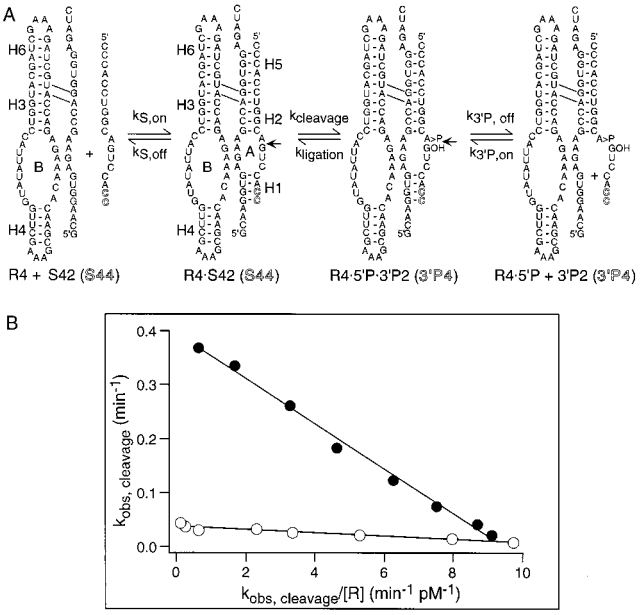

FIGURE 2: Cleavage activity of a hairpin ribozyme with a four-way helical junction. (A) Substrate cleavage reactions include substrate binding, cleavage, and product dissociation steps and, in the reverse direction, product binding, ligation, and substrate dissociation steps. Intramolecular helices H3, H4, and H6 and loop B form within R4 RNA. Intermolecular helices H1, H2, and H5 and loop A form upon substrate binding. 5′ product RNA associates with the ribozyme through H2 and H5 while 3′ product RNA associates with the ribozyme through H1. S42 and 3′P2 RNAs form H1 sequences with two base pairs. S44 and 3′P4 RNAs form H1 sequences with two additional base pairs (outline font). (B) Eadie−Hofstee plots of the ribozyme concentration dependence of $k_{obs,cleavage}$. Rate constants of 0.45 ± 0.023 and 0.036 ± 0.0014 min^{-1} were determined from *y*-intercepts for R4-mediated cleavage of S42 (●) and S44 (○), respectively. K_M^S values of 48 ± 4 nM for S42 and 2.7 ± 0.3 nM for S44 were determined from the slopes.

substrate binding. Two cleavage substrates, S42 and S44, are identical except for 3′ terminal nucleotides that participate in forming H1, the intermolecular helix that joins the ribozyme and the 3′ cleavage product (Figure 2A). S42 associates with the ribozyme to form an H1 sequence with two base pairs. Two additional 3′ terminal cytosine residues allow S44 to form four base pairs in H1 (Figure 2A, shadow font).

S44 cleaves with a rate constant of 0.036 min^{-1} and a K_M^S value of 2.7 nM (Figure 2B, open circles). These kinetic parameters are about 10-fold below the rate constant of ∼0.3 min^{-1} and the K_M^S value of ∼30 nM that are typical of intermolecular cleavage reactions with minimal hairpin ribozymes under similar conditions (*5*). The low rate constant for S44 cleavage is similar, however, to the cleavage rate of 0.038 min^{-1} recently reported for another hairpin ribozyme variant that also contains a four-way helical junction (*22*).

In intermolecular reactions with minimal hairpin ribozymes under standard conditions, ligation is ∼10-fold faster than cleavage when the ribozyme is saturated with cleavage products (*5*). The 5′ product associates with minimal ribozymes to form the H2 helix with only four base pairs (Figure 1A). Consequently, concentrations that are saturating for substrate binding typically are far below saturation for binding of the 5′ cleavage product, and cleavage is driven by rapid dissociation and dilution of 5′ cleavage products (*5*). Cleavage is driven by rapid 5′ product dissociation even when 3′ products remain bound in stable H1 sequences with

as many as eight base pairs (*5*). Due to the presence of four additional intermolecular base pairs in the H5 sequence of R4, however, 5′ product RNAs are expected to bind R4 with much higher affinity and dissociate much more slowly than 5′ products that bind to minimal ribozymes through the H2 helix alone. The slow rate observed for R4 cleavage of S44 could be explained if both 5′ and 3′ cleavage products dissociate at rates that are slower than or on the same order as ligation rates. If this is the case, a significant fraction of cleavage events would be followed by rapid re-ligation of bound products, causing observed cleavage rates to fall (Figure 2A).

To learn whether slow product release limits observed S44 cleavage rates, cleavage reactions were carried out with a second substrate, S42, that forms an H1 sequence with two fewer base pairs. Calculations based on empirically determined free energy parameters for RNA helices (*31*) show that the loss of two base pairs from the H1 sequence reduces product binding affinity by ~5.7 kcal/mol and accelerates product dissociation more than 15 000-fold (*5*). If slow cleavage of S44 results from partitioning of cleavage products between dissociation and re-ligation, 3′P42 could dissociate fast enough to avoid re-ligation, causing observed cleavage rates to rise. Consistent with this prediction, cleavage reactions with R4 and S42 display more typical kinetic parameters with a $k_{cleavage}$ value of 0.45 min^{-1} and a K_M^S value of 48 nM (Figure 2B, closed circles).

A pulse−chase experiment was carried out to confirm that a hairpin ribozyme with four base pairs in H1 is not catalytically impaired and that products of S44 cleavage undergo rapid ligation (Figure 3). First, R4 and [5′-^{32}P]S42 were combined to initiate a cleavage reaction. After cleavage of [5′-^{32}P]S42 was nearly complete, 3′P4, the 3′ product of S44 cleavage, was added (Figure 3A). Within minutes, virtually all of the ^{32}P present in the 5′ product of S42 cleavage was converted to [5′-^{32}P]S44, the product of 3′P4 ligation (Figure 3B). Despite the low cleavage activity detected with S44, therefore, the R4·5′P·3′P4 complex is highly active in a ligation reaction.

Self-Cleavage Kinetics. If slow S44 cleavage kinetics reflect inhibition of cleavage through re-ligation of bound product and not a defect in catalysis, ribozymes with two-way and four-way helical junctions should display similar cleavage kinetics when 3′ products dissociate at rates that are much faster than ligation rates. Self-cleavage kinetics were compared directly for ribozymes with four-way and two-way helical junctions using ribozyme configurations in which the 5′ cleavage product RNA is covalently joined to 5′ ribozyme RNA (Figure 4A,B). 5′R2 has the same H1, H2, H3, and H4 sequences as 5′R4, but the H5 and H6 sequences of 5′R4 are replaced by an unstructured oligonucleotide linker in 5′R2. The self-cleaving configuration prevents differences in 5′ cleavage product binding affinity from obscuring effects of 3′ product dissociation on observed cleavage rates.

Self-cleaving ribozymes, [α-^{32}P]LR24 and [α-^{32}P]LR43, were first prepared in ligation reactions with [α-^{32}P]5′R2 and 3′P4 or with [α-^{32}P]5′R4 and 3′P3. Ligation reactions were then diluted, and the amount of [α-^{32}P]5′R2 or [α-^{32}P]5′R4 was measured over time. LR24 and LR43 self-cleaved at virtually identical rates of 0.52 and 0.63 min^{-1}, respectively (Figure 4C). These self-cleavage rates are similar to the

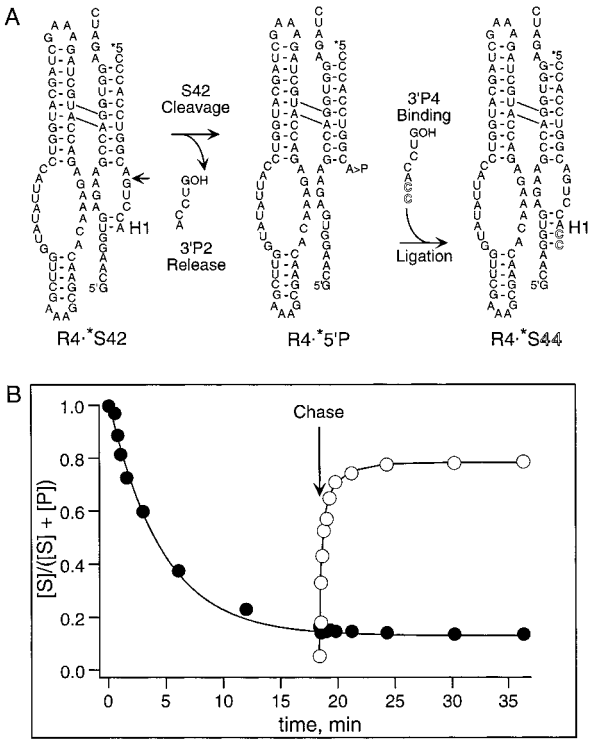

FIGURE 3: Pulse−chase experiment demonstrates that 3′P4 undergoes rapid ligation. (A) Reaction scheme used to monitor activity of the R4·5′P·3′P4 complex. The reaction was initiated by combining R4, at a concentration of 500 nM, with a trace amount (0.1 nM) of [5′-^{32}P]S42. After 18 min, 3′P4 RNA was added at a final concentration of 750 nM, and ligation activity was monitored from the appearance of [5′-^{32}P]S44 over time. Asterisks indicate the [5′-^{32}P] label. (B) The amounts of [5′-^{32}P]S42 (●) and [5′-^{32}P]S44 (○) are shown as a function of time. Lines represent calculated fits. The fit calculated for [S42]/([S42] + [S44] + [5′P]) = $e^{-k_{obs,cleavage}t}$ gives k_{obs} = 0.14 ±0.007 for S42 cleavage. The appearance of S44 over time was best fit by a double exponential equation for which individual parameters are poorly defined.

cleavage rate constant of 0.45 min^{-1} measured for intermolecular cleavage reactions with R4 and S42 but are much faster than the intermolecular cleavage rate constant of 0.036 min^{-1} measured for R4 cleavage of S44 (Figure 2). The H1 sequence formed by 3′P3 binding is more stable than the H1 sequence formed by 3′P2 binding by ~2 kcal/mol (*31*) so that product dissociation rates for 3′P2 and 3′P3 are expected to differ almost 40-fold. The observation that R4·S42 and LR43 cleave at virtually identical rates suggests that product dissociation is much faster than ligation in both cases and that the cleavage step and not slow product dissociation is rate-determining. Evidently, ribozymes with two- or four-way helical junctions self-cleave at the same rates when the weak affinity of the ribozyme for 3′ products allows rapid product dissociation. Therefore, it appears that re-ligation of bound 3′P4 accounts for the low rate constant observed for R4 cleavage of S44.

This experiment also demonstrates that the same product, 3′P4, that appears to undergo re-ligation in reactions with R4 dissociates before re-ligation in reactions with 5′R2. The difference in partitioning of 3′P4 between dissociation and ligation could be explained if ligation is faster or if product dissociation is slower for ribozymes with a four-way helical junction compared to minimal ribozymes. The following experiments were designed to test each possibility.

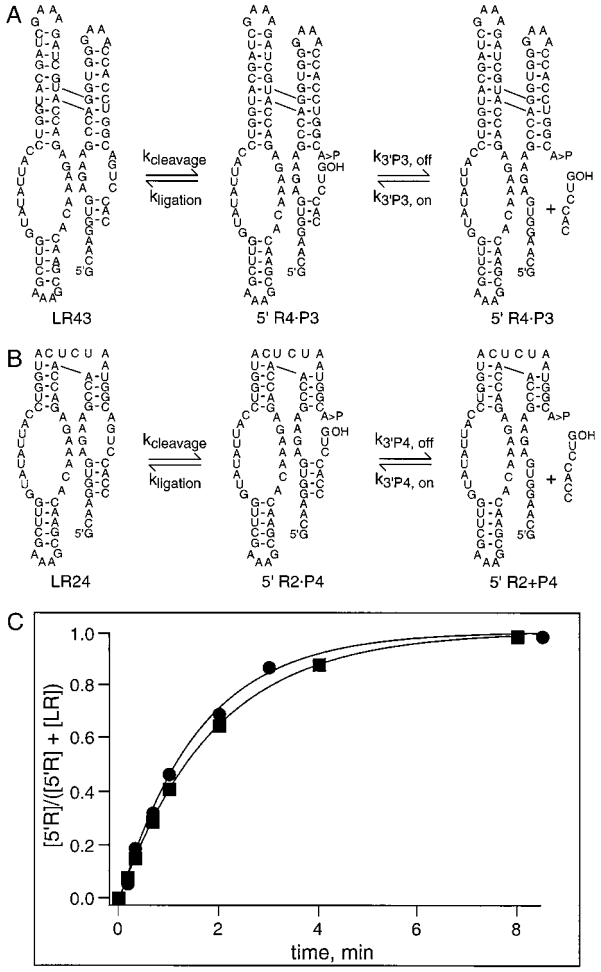

FIGURE 4: (A) LR43 self-cleavage reaction. (B) LR24 self-cleavage reaction. (C) Self-cleavage rates of 0.63 ± 0.02 and 0.52 ± 0.01 min^{-1} were determined for LR43 (●) and LR24 (■), respectively, from the fit to $[LR]/([5'R{\cdot}P] + [LR]) = e^{-k_{cleavage}t}$ after normalization to the fraction of ligated ribozyme at the start of the cleavage reaction.

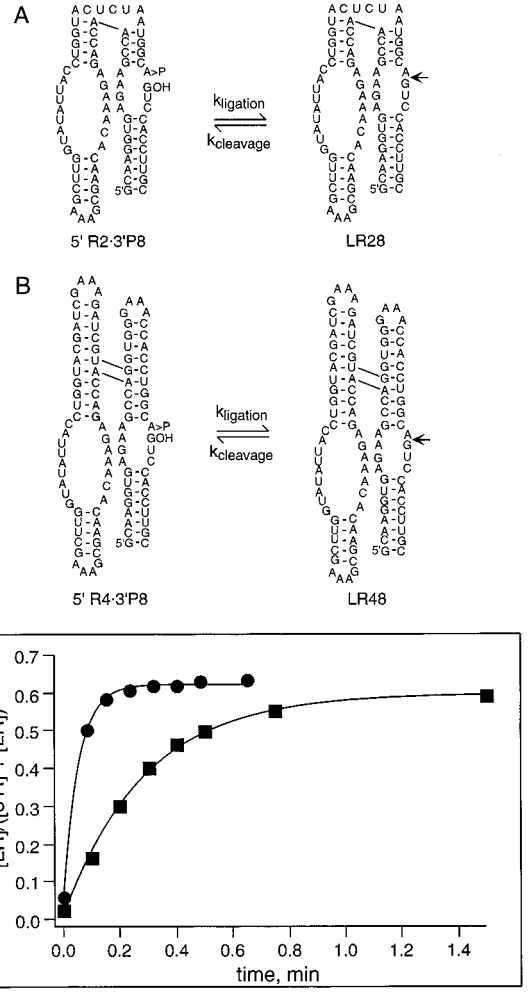

FIGURE 5: Self-ligation rates were measured for ribozymes with two-way or four-way junctions that have the same H1 sequence containing eight base pairs. Observed ligation rates represent the rate of approach to the equilibrium between ligation and cleavage and equal the sum of ligation and cleavage rate constants. (A) Self-ligation of 5′R2 and 3′P8, forms LR28. (B) Self-ligation of 5′R4 and 3′P8, forms LR48. (C) $k_{obs,ligation}$ values of 3.5 ± 0.2 and 18 ± 0.8 min^{-1} were calculated for 5′R2·3′P8 (■) and 5′R4·3′P8 (●), respectively, from the fit to $[LR]/([5'R{\cdot}P] + [LR]) = e^{-k_{obs,ligation}t}$.

Self-Ligation Kinetics. Self-ligation kinetics were compared in reactions with 5′R2 or 5′R4 and a large 3′ product RNA, 3′P8, that associates with 5′ ribozyme RNA to form an H1 sequence with eight base pairs (Figure 5A,B). A trace amount of [α-^{32}P]5′R2 or [α-^{32}P]5′R4 was first combined with a high concentration of 3′P8 under conditions that promote complete saturation of [α-^{32}P]5′R with 3′P8 but support no detectable ligation. Virtually no dissociation of the stable [α-^{32}P]5′R·3′P8 complex is expected to occur on the time scale of ligation reactions (*25*). After dilution of the [α-^{32}P]5′R·3′P8 complex into reaction buffer, observed ligation rates of 3.5 and 18 min^{-1} were determined from the appearance of [α-^{32}P]LR28 or [α-^{32}P]LR48, respectively, over time (Figure 5C).

The 5′R·3′P8 complex undergoes ligation in a reaction that approaches equilibrium at a rate that is the sum of the cleavage and ligation rate constants (eq 1).

$$k_{obs,ligation} = k_{ligation} + k_{cleavage} \quad (1)$$

A rate constant of 2.9 min^{-1} can be calculated for 5′R2 self-ligation from the difference between the measured self-cleavage rate of 0.52 min^{-1} and the observed self-ligation rate of 3.5 min^{-1}. The same calculation gives a 5′R4 self-ligation rate constant of 17.6 min^{-1}. Thus, self-ligation of a hairpin ribozyme with a four-way helical junction is 6-fold faster than self-ligation of a minimal hairpin ribozyme.

$$K_{eq}^{int} = k_{ligation}/k_{cleavage} \quad (2)$$

Calculation of K_{eq}^{int} values from the ratio of ligation and cleavage rate constants (eq 2) shows that a self-cleaving hairpin ribozyme with a four-way helical junction favors ligation over cleavage by nearly 30-fold while a minimal self-cleaving hairpin favors ligation by less than 6-fold under the same conditions. Thus, the balance between 3′ product dissociation and ligation shifts in favor of ligation for ribozymes in the context of a four-way helical junction.

Provided that the highest activation barrier encountered during ligation and cleavage reactions is the same, the ratio of ligation and cleavage rate constants (eq 2) will equal the ratio of ligated ribozyme and 5′ ribozyme−product complex, [LR]/[5′R·P], when a ligation reaction at saturating concentrations has reached equilibrium. In practice, correspondence between K_{eq}^{int} values calculated from eq 2 and values

calculated from the fraction of ligated ribozyme at the end of a ligation reaction is difficult to confirm experimentally. Under most conditions, some fraction of 5′ ribozyme RNA is catalytically inactive, likely due to misfolding of RNAs into catalytically inactive conformations (*32*, *33*) or to hydrolysis of the 2′,3′-cyclic phosphate during purification of the 5′ ribozyme fragment. Consequently, calculations based on the fraction of ligated ribozyme at equilibrium give lower values for K_{eq}^{int} because the measured amount of 5′R includes catalytically inactive RNA (*25*). The average values of 0.7 for the fraction of LR48 and 0.6 for the fraction of LR28 at equilibrium in ligation reactions with saturating concentrations of 3′P8 give values of 2.3 and 1.5 for [LR48]/[5′R4·3′P8] and [LR28]/[5′R4·3′P8], respectively. Equilibrium constants calculated in this way are much lower than the values of 30 and 6 that are obtained from ligation and cleavage rate constants for 5′R4 and 5′R2, respectively, using eq 2. This discrepancy can be explained if 26% of 5′R4 and 5′R2 RNAs are assumed to be catalytically inactive.

Stability of Ribozyme−3′ Product Complexes. The interaction between the ribozyme and 3′ product RNAs defines essential features of the catalytically active ribozyme structure. Binding of 3′ product RNA generates loop A and the intermolecular H1 sequence (Figure 4). A $G_{+1}A$ substitution of the 5′ terminal guanosine of the 3′ product RNA eliminates detectable catalytic activity and interferes with docking (*20*, *23*, *34*), pointing to a critical role for this nucleotide in ribozyme assembly and catalysis.

Self-ligation is the reverse of the self-cleavage reaction diagrammed in Figure 4. The extent of ligation at the end of the reaction is the product of the binding equilibrium and the equilibrium between ligation and cleavage, K_{eq}^{int}. Apparent equilibrium dissociation constants for 5′R·3′P complexes, $K_{d,app}^{3'P}$, can be calculated from the 3′ product RNA concentration dependence of the extent of ligation at equilibrium (Figure 6).

With 3′ product RNA in large excess over [α-^{32}P]5′R so that [3′P] ≅ $[3'P]_{total}$ throughout a ligation reaction, the fraction of ligated ribozyme, LR, at equilibrium depends on the concentration of 3′ product RNA according to eq 3.

$$\frac{[LR]}{[LR]+[5'R]} = \frac{[3'P]}{K_{d,app}^{3'P} + [3'P]} \qquad (3)$$

For the simple mechanism shown in Figure 4, the apparent equilibrium dissociation constant, $K_{d,app}^{3'P}$, is the product of the binding equilibrium, $k_{off}^{3'P}/k_{on}^{3'P}$, and the internal equilibrium between ligation and cleavage of bound 3′ product, K_{eq}^{int} (eq 4).

$$K_{d,app}^{3'P} = \frac{k_{off}^{3'P}}{k_{on}^{3'P}} \frac{k_{cleavage}}{k_{ligation}} = \frac{K_d^{3'P}}{K_{eq}^{int}} \qquad (4)$$

An apparent equilibrium dissociation constant, $K_{d,app}^{3'P4}$, of 5 nM was measured in self-ligation reactions with 5′R4 and 3′P4 (Figure 4A,B, Figure 6B, Table 1). Factoring out the contribution of K_{eq}^{int} (eq 4) using the value of 30 that is obtained from the ratio of ligation and cleavage rate constants (eq 2) gives an equilibrium dissociation constant of 140 nM. This value represents a weighted average of the equilibrium binding of 3′P4 to 5′R4 in both docked and undocked

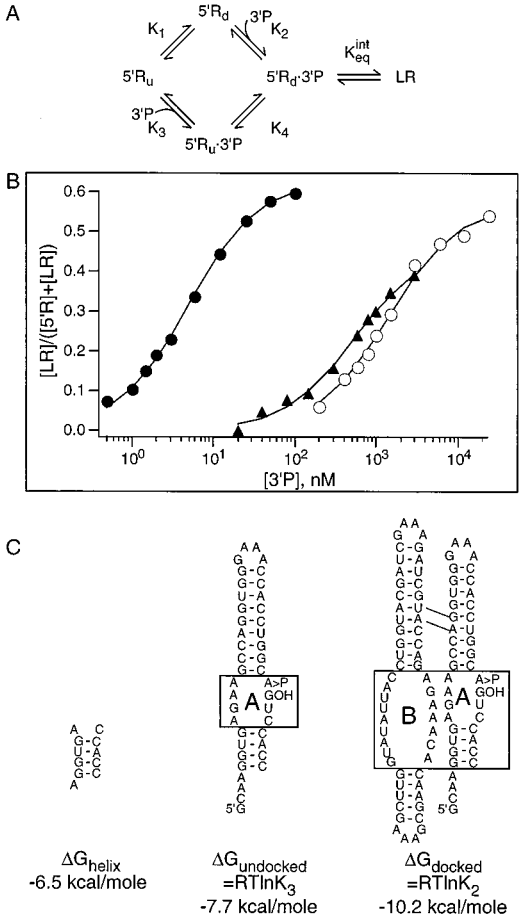

FIGURE 6: Equilibrium dissociation constants for 5′R·3′P complexes determined from the 3′P concentration dependence of the extent of ligation at equilibrium. (A) A thermodynamic framework for analysis of the 3′ product binding reaction includes the equilibrium between docked and undocked 5′R ($K_1 = [5'R_{undocked}]/[5'R_{docked}]$), product binding and dissociation from 5′R RNA in both docked ($K_2 = [5'R_{docked}][3'P]/[5'R_{docked}\cdot 3'P]$) and undocked ($K_3 = [5'R_{undocked}][3'P]/[5'R_{undocked}\cdot 3'P]$) conformations, the equilibrium between docked and undocked 5′R·3′P complexes ($K_4 = [5'R_{undocked}\cdot 3'P]/[5'R_{docked}\cdot 3'P]$), and the equilibrium between LR and the docked 5′R·3′P complex ($K_{eq}^{int} = [LR]/[5'R_{docked}\cdot 3'P]$). (B) Apparent equilibrium dissociation constants of 1400 ± 90, 5.0 ± 0.17, and 550 ± 53 nM were determined for 5′R2·3′P4 (○), 5′R4·3′P4 (●), and 5′R4·3′P3 (▲) complexes, respectively, from the fit to fraction $LR_{t=\infty} = (LR_{sat})([5'R\cdot 3'P]/([5'R\cdot 3'P] + K_{d,app}^{3'P})$ where $LR_{t=\infty}$ is the fraction of ligated ribozyme at equilibrium and LR_{sat} is the fraction of ligated ribozyme at equilibrium with a saturating concentration of 3′P. (C) The change in free energy expected for formation of a simple RNA helix with the same sequence as the intermolecular helix formed between ribozymes and cleavage products, H1, was calculated using empirically determined free energy parameters for RNA helix formation (*31*), giving a ΔG_{helix} value of −6.5 kcal/mol for the H1 sequence of the 5′R·3′P4 complex. $\Delta G_{25°C,undocked} = RT \ln K_3 = -7.7$ kcal/mol reflects binding energy derived from base-pairing interactions and tertiary interactions within the undocked complex. Therefore, the difference between $\Delta G_{25°C,undocked}$ and ΔG_{helix} can be used to estimate that extrahelical interactions within the H1−loop A−H2 domain of the 5′R·3′P4 complexes contribute ∼−1.2 kcal/mol to product binding energy. $\Delta G_{25°C,docked} = RT \ln K_2 = -10.2$ kcal/mol reflects binding energy derived from tertiary interactions within the docked complex. The difference between $\Delta G_{25°C,docked} = RT \ln K_2$ −10.2 kcal/mol and $\Delta G_{25°C,undocked} = RT \ln K_3 = -7.7$ kcal/mol gives a coupling energy, $\Delta\Delta G_{25°C} = -2.5$ kcal/mol, for the energy contributed to 3′ product binding by interactions that form within the docked, but not the undocked, 5′R4·3′P4 complex.

Table 1: Stability of 5′ Ribozyme−3′ Product Complexes

complex	$K_{d,app}^{3'P}$ (nM)[a]	$K_d^{3'P}$ (nM)[b]	$\Delta G_{25°C}$[c]	$\Delta G_{25°C,d}$[d]	$\Delta G_{25°C,u}$[e]	$\Delta\Delta G_{25°C,d-u}$[f]	$\Delta G_{25°C,helix}$[g]	$\Delta\Delta G_{25°C,u-h}$[h]
5′R4·3′P3	550 ± 50	2500	−7.7	−7.4	−4.9	−2.5	−2.9	−1.0
5′R4·3′P4	5.0 ± 0.2	140	−9.4	−10.2	−7.7	−2.5	−6.5	−1.2
5′R2·3′P4	1400 ± 90	7800	−7.0	−	−	−	−6.5	−

[a] Apparent equilibrium dissociation constants were measured from the 3′P concentration dependence of ligation reaction extents (Figure 6), as described in the text. [b] Calculated from $K_{d,app}^{3'P} \times K_{eq}^{int}$ (eq 4). [c] Calculated from $\Delta G = RT \ln (K_d^{3'P})$, where R is the gas constant, T is the temperature in degrees kelvin, and $K_d^{3'P} = K_{d,app}^{3'P} \times K_{eq}^{int}$. [d] Calculated from $\Delta G = RT \ln (K_2)$, where $K_2 = [5'R_{docked}][3'P]/[5'R\cdot3'P_{docked}]$, as described in the text. [e] Calculated from $\Delta G = RT \ln (K_3)$, where $K_3 = [5'R_{undocked}][3'P]/[5'R\cdot3'P_{undocked}]$, as described in the text. [f] Calculated from the difference between $\Delta G_{25°C,d}$ and $\Delta G_{25°C,u}$. [g] Calculation based on empirically determined free energy parameters for formation of base-paired RNA helices (*31*). [h] Calculated from the difference between $\Delta G_{25°C,u}$ and $\Delta G_{25°C,helix}$.

conformations (Table 1). An apparent equilibrium dissociation constant, $K_{d,app}^{3'P4}$, of 1400 nM was measured in self-ligation reactions with the minimal ribozyme, 5′R2, and 3′P4 (Figure 4B, Figure 6B, Table 1). Using eq 4 and the K_{eq}^{int} value of 6 calculated from eq 2, an equilibrium dissociation constant of 7800 nM can be calculated for 3′P4 binding to the minimal 5′R2 ribozyme (Table 1). This value is more than 50-fold higher than the equilibrium dissociation constant calculated for binding of the same 3′ product RNA to 5′R4.

FRET experiments recently have provided evidence that the hairpin ribozyme is in equilibrium between an active docked conformation and an inactive extended form (*19*−*23*). Therefore, a complete thermodynamic framework for analysis of the 3′ product binding reaction includes the equilibrium between docked and undocked 5′R, 3′ product binding and dissociation from 5′R in both docked and undocked conformations, the equilibrium between docked and undocked 5′R·3′P complexes, and the equilibrium between LR and the docked 5′R·3′P complex (Figure 6A). For this detailed mechanism, it can be shown that

$$\frac{[LR]}{[LR]+[5'R]} = \frac{[3'P]}{\frac{(1+K_1)K_2}{K_{eq}^{int}} + \left(\frac{K_4}{K_{eq}^{int}} + \frac{1}{K_{eq}^{int}} + 1\right)[3'P]} \quad (5)$$

Docking equilibria have been quantitated for a series of hairpin ribozyme variants with different helical junctions using time-resolved FRET (*23*). Direct application of docking equilibria measured using FRET to interpretation of functional assays described here is limited by differences in ribozyme sequences and the lower temperature of 17.8 °C that was used for FRET assays. Even so, FRET measurements of the relative stabilities of docked and undocked conformations of different hairpin ribozyme variants can be used to estimate the relative contributions of interactions within docked and undocked 5′R·3′P complexes to 3′ product binding.

Analysis of reaction kinetics presented here and physical characterization of docking equilibria using time-resolved FRET (*23*) suggest that the second term in the denominator of eq 5 reduces to [3′P]. The first part of this term, K_4/K_{eq}^{int}, becomes important only when K_4 is large, that is, when the undocked form of the 5′R·3′P complex predominates over the docked form. FRET studies give a small K_4 value of 0.05 for a self-cleaving ribozyme with a four-way helical junction that resembles the 5′R4·3′P complex (*23*). Assuming a K_4 value of 0.05 and a K_{eq}^{int} value of 30, the value measured for the 5′R4 self-ligation reaction (Figure 5), the value of K_4/K_{eq}^{int} is 0.0017. Even if FRET measurements greatly overestimate the relative stability of the docked conformation of the 5′R·3′P complex and the actual K_4 value is as high as 1, the contribution of this term would still be small, less than 0.033. Likewise, the second part of this term, $1/K_{eq}^{int}$, is significantly less than 1. Therefore, $K_{d,app}^{3'P}$ is determined primarily by the first term in the denominator of eq 5 (eq 6).

$$K_{d,app}^{3'P} \approx \frac{(1+K_1)K_2}{K_{eq}^{int}} \quad (6)$$

The magnitude of K_1, the equilibrium distribution of docked and undocked conformations of 5′R4, can be estimated from time-resolved FRET measurements of a ribozyme with a four-way helical junction similar to R4 (Figure 2A) (*23*). In the absence of bound substrate, this ribozyme displayed a K_1 value of 3.4. By assuming a value of 3.4 for K_1 and a value of 30 for K_{eq}^{int}, a value of 34 nM can be calculated for K_2, the equilibrium dissociation constant for 3′P4 binding to docked 5′R4. This corresponds to a free energy of −10.2 kcal/mol for 3′ product binding within the docked 5′R4·3′P4 complex (Table 1). Because the H2 and H5 sequences form in the absence of 3′ product but not in the absence of substrate, FRET measurements of the docking equilibrium for ribozyme in the absence of substrate likely overestimate K_1 for docking of 5′R4. If virtually all of 5′R4 is in the docked conformation at equilibrium so that K_1 is overestimated by as much as 10-fold, $K_d^{3'P4,docked}$ values would increase by only ∼3-fold, leading to an error of ∼−0.5 kcal/mol in the calculated binding energy. Conversely, if virtually no 5′R4 is docked at equilibrium, underestimation of K_1 results in a proportional error in the calculated K_2 value.

Based on the thermodynamic cycle shown in Figure 6A and eq 7, a value of 2300 nM can be calculated for K_3, the equilibrium dissociation constant for 3′P4 binding to the undocked conformation of 5′R4, from K_1, K_2, and K_4 values. Thus, interactions within the undocked complex contribute −7.7 kcal/mol to the 3′P4 binding energy (Table 1, Figure 6C).

$$K_1K_2 = K_3K_4 \quad (7)$$

The difference between $\Delta G_{25°C,docked} = RT \ln K_2 = -10.2$ kcal/mol and $\Delta G_{25°C,undocked} = RT \ln K_3 = -7.7$ kcal/mol gives a coupling energy, $\Delta\Delta G_{25°C} = -2.5$ kcal/mol, for the energy contributed to 3′ product binding by interactions that form within the docked, but not the undocked, 5′R4·3′P44 complex (Table 1, Figure 6C). Conversely, binding of 3′P44 stabilizes docking by the same amount.

The H1 sequence of the 5′R4·3′P3 complex contains one fewer G:C base pair than the H1 sequence of the 5′R4·3′P4

complex (Figure 4A,B). An apparent equilibrium dissociation constant, $K_{d,app}^{3'P3}$, of 550 nM was measured in self-ligation reactions with 5′R4 and 3′P3 (Figure 4A, Figure 6B, Table 1). The same series of calculations gives $\Delta G_{25°C,docked} = -7.4$ kcal/mol and $\Delta G_{25°C,undocked} = -4.9$ kcal/mol for binding of 3′P3 to 5′R4 and the same coupling energy, $\Delta\Delta G_{25°C} = -2.5$ kcal/mol, for the energy contributed by docking to 3′P43 binding energy (Table 1).

The change in free energy expected for formation a simple RNA helix with the same sequence as the intermolecular helix formed between ribozymes and cleavage products, H1, can be calculated using empirically determined free energy parameters for RNA helix formation (*31*). These calculations give ΔG_{helix} values of −2.9 and −6.5 kcal/mol for the H1 sequences of the 5′R·3′P3 and 5′R·3′P4 complexes, respectively (Table 1). $\Delta G_{25°C,undocked}$ reflects binding energy derived from base-pairing interactions and tertiary interactions within the undocked complex. Although the uncertainty in this estimate is high, the difference between $\Delta G_{25°C,undocked}$ and ΔG_{helix} can be used to estimate that extrahelical interactions within the H1−loop A−H2 domain of 5′R·3′P3 and 5′R·3′P4 complexes contribute ∼−1 kcal/mol to binding energy (Table 1, Figure 6C).

A potential source of error in these calculations is uncertainty in the value of K_{eq}^{int}. Error in the value of K_{eq}^{int} creates the same proportional error in both K_2 and K_3 but has no effect on the calculated free energy difference between docked and undocked 5′R·3′P complexes. Based on similarity between ligation and docking rates, it has been suggested that the docking step is rate-determining for hairpin ribozyme-mediated ligation (*20*). However, the activation energy of 28.8 kcal/mol reported for docking (*20*) is significantly higher than the activation energy of 13 kcal/mol measured for self-ligation of a similar minimal ribozyme sequence under the same conditions (*25*). The difference in activation energies for docking and ligation suggests that a step other than docking presents the highest energy barrier to ligation. Resolving this discrepancy will require direct comparison of docking and ligation kinetics with the same ribozyme sequences under identical conditions. If measured $k_{ligation}$ values do reflect a slow docking step, however, and not the rate at which the docked 5′R·3′P complex undergoes ligation as shown in Figure 6A, actual K_{eq}^{int} values would be higher than 30, the value obtained from the ratio of ligation and cleavage rate constants (eq 2). If this is the case, product binding energies would be overestimated in these calculations. For example, using the 10-fold higher K_{eq}^{int} value of 300, $\Delta G_{25°C,docked}$ and $\Delta G_{25°C,undocked}$ values each increase by 1.4 kcal/mol to −8.8 and −6.3 kcal/mol, respectively. Alternatively, actual K_{eq}^{int} values might be lower than the values obtained from ligation and cleavage rate constants (eq 2) if the rate-determining steps for ligation and cleavage are not the same. Using a 10-fold lower K_{eq}^{int} value of 3, $\Delta G_{25°C,docked}$ and $\Delta G_{25°C,undocked}$ values each decrease by 1.4 kcal/mol to −11.6 and −9.1 kcal/mol, respectively. Regardless of the actual value of K_{eq}^{int}, however, the difference between $\Delta G_{25°C,docked}$ and $\Delta G_{25°C,undocked}$ values remains −2.5 kcal/mol.

A K_4 value of 0.34 can be estimated from the equilibrium distribution of docked and undocked ribozymes with a bulged two-way helical junction similar to 5′R2 that was determined using time-resolved FRET (*23*). However, detailed analysis of product binding energy also requires an estimate of the relative stability of docked and undocked 5′R2 in the absence of bound 3′P, and this information is not yet available. In the absence of bound substrate, no docking was detected for a minimal ribozyme with the structure of R2, suggesting that the value of K_1 is high enough to contribute significantly to $K_{d,app}^{3'P4}$ (*20*, *23*).

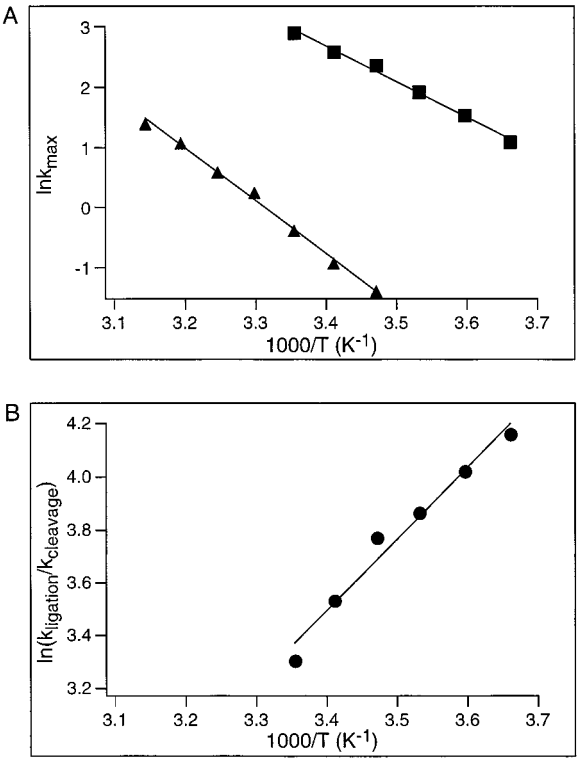

FIGURE 7: Temperature dependence of cleavage and ligation in 50 mM NaHEPES, pH 7.5, 10 mM $MgCl_2$, 0.1 mM EDTA. (A) Arrhenius plot of the temperature dependence of the rate constants for ligation (■) and cleavage (▲) gives values for the activation energy, E_a, of 12 ± 0.5 and 17 ±0.8 kcal/mol, respectively. (B) van't Hoff plot, using K_{eq}^{int} values obtained from the ratio of ligation and cleavage rate constants, gives $\Delta H° = -5.4 \pm 0.4$ kcal/mol and $\Delta S° = -11 \pm 2$ eu.

Temperature Dependence of Cleavage and Ligation. LR43 self-cleavage rate constants increased from 0.25 min^{-1} at 15 °C to 4 min^{-1} at 45 °C. Slow 3′P3 dissociation prevented direct self-cleavage rate measurements at temperatures below 15 °C. Self-ligation rate constants increased from 3 min^{-1} at 0 °C to 18 min^{-1} at 25 °C and became too fast to measure at temperatures above 25 °C. To allow calculation of self-ligation rates at temperatures between 0 and 15 °C, cleavage rate constants were extrapolated from the temperature dependence of cleavage rate constants that were measured at higher temperatures. Arrhenius plots of these data (Figure 7A) give activation energies, E_a, of 12 and 17 kcal/mol for ligation and cleavage reactions, respectively. The linearity of these plots suggests that no change in the rate-determining step occurs at low temperatures and that the use of extrapolated cleavage rate constants for calculation of ligation rate constants led to no significant errors. Thermodynamic activation parameters calculated from E_a values, reflecting differences between ground state and transition state energies for ligated ribozyme and for the 5′ ribozyme−3′ product complex, are shown in Table 2.

Table 2: Thermodynamic Parameters for Ribozyme-Catalyzed Cleavage and Ligation[a]

	cleavage			ligation			K_{eq}^{int} [f]		
ribozyme	$\Delta G^{\ddagger}$ [c]	$\Delta H^{\ddagger}$ [d]	$\Delta S^{\ddagger}$ [e]	$\Delta G^{\ddagger}$ [c]	$\Delta H^{\ddagger}$ [d]	$\Delta S^{\ddagger}$ [e]	$\Delta G°$	$\Delta H°$	$\Delta S°$
LR4	20 ± 0.02	17 ± 0.8	-11 ± 3	18 ± 0.4	11 ± 0.5	-24 ± 2	-2.0	-5.4 ± 0.5	-11 ± 2
LR2[b]	20 ± 0.5	17 ± 1.0	-11 ± 3	20 ± 0.5	12 ± 1	-25 ± 3	-0.5	-4.5 ± 0.3	-14 ± 1

[a] Calculated for $T = 298$ K (25 °C). $\Delta G°$ and $\Delta H°$ are kcal/mol. $\Delta S°$ are eu. [b] Taken from Nesbitt et al. (*25*). [c] Calculated from $\Delta G^{\ddagger} = -RT \ln(k_{max}h/k_BT)$ where h is Planck's constant, k_B is Boltzmann's constant, and k_{max} is the rate constant for self-cleavage or ligation at $T = 298$ K. Values represent the mean and range of two or more measurements. [d] Calculated from $\Delta H^{\ddagger} = E_a - RT$. Errors were computed from fits to Arrhenius plots. [e] Calculated from $\Delta G^{\ddagger} = \Delta H^{\ddagger} - T\Delta S^{\ddagger}$. [f] K_{eq}^{int} values calculated from the ratio of self-ligation and self-cleavage rate constants. Thermodynamic parameters calculated from van't Hoff plots using $\Delta G° = \Delta H° - T\Delta S°$.

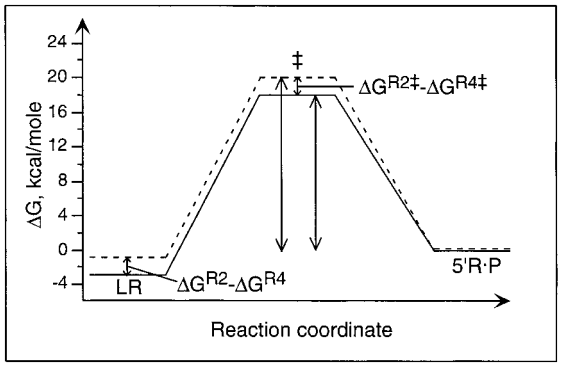

FIGURE 8: Free energy diagram illustrating the difference between reactions catalyzed by a minimal hairpin ribozyme (dashed lined) and a hairpin ribozyme in the context of a four-way helical junction (solid line). The four-way helical junction stabilizes ligated ribozyme and the transition state relative to the 5′ ribozyme−product complex so that the activation barrier to ligation decreases while the activation barrier to cleavage remains unchanged.

Ligation was favored relative to cleavage throughout the temperature range that was tested although the preference for ligation decreased with increasing temperature. K_{eq}^{int} values calculated from the ratios of ligation and cleavage rate constants, $k_{ligation}/k_{cleavage}$, ranged from 64 at 0 °C to 27 at 25 °C. A van't Hoff plot of K_{eq}^{int} values (Figure 7B) gives $\Delta H° = -5.4$ kcal/mol and $\Delta S° = -11$ eu for the differences in enthalpy and entropy between the 5′ ribozyme−product complex and ligated ribozyme. Thus, a negative (favorable) enthalpy overcomes a negative (unfavorable) entropy to drive the reaction toward ligation over a broad range of temperatures.

DISCUSSION

In the natural context of a four-way helical junction, hairpin ribozyme reactions exploit a kinetic mechanism that is distinct from the mechanism of minimal hairpin ribozymes. The four-way junction ribozyme is a particularly efficient RNA ligase. At 25 °C, self-ligation of 5′R4 is 6-fold faster than self-ligation of 5′R2, and self-ligation of 5′R4 becomes too fast to measure directly at higher temperatures. A self-ligation rate of 40 min^{-1} at 37 °C can be extrapolated from the temperature dependence of ligation, and ligation rates are expected to exceed 1 s^{-1} at temperatures above 45 °C. The difference between ligation rate constants for ribozymes with two-way or four-way helical junctions demonstrates that stabilization of the docked conformation lowers the activation barrier for ligation by ~ 2 kcal/mol (Table 2, Figure 8).

In contrast to the significant acceleration of ligation, self-cleavage rates are unaffected by junction structure provided that 3′ product dissociation is much faster than ligation and is irreversible. The cleavage rate constant of 0.45 min^{-1} observed for intermolecular cleavage of S42 by R4 and the LR43 self-cleavage rate of 0.63 min^{-1} are similar to the LR24 self-cleavage rate measured in parallel experiments and to rate constants previously measured for intermolecular reactions of minimal hairpin ribozymes under similar conditions (*5*, *35*). Evidently, the additional stability of the docked hairpin conformation in the context of a four-way helical junction has little effect on the activation barrier for cleavage (Table 2, Figure 8). Thus, the context of a four-way helical junction appears to decrease the free energy difference between the 5′ ribozyme complex and the transition state and stabilize ligated ribozyme relative to the 5′ ribozyme complex by about the same amount (Figure 8).

Because self-cleavage occurs at virtually identical rates for hairpin ribozymes with two-way or four-way helical junctions, the ratio of ligation and cleavage rate constants changes from less than 6 for a minimal ribozyme to nearly 30. We previously found that high concentrations of cations shift the internal equilibrium toward ligated ribozyme by accelerating ligation and not by slowing cleavage (*25*). Thus, tertiary structure stabilization by the context of a four-way helical junction mimics the effect of high cation concentrations. The observation that both reaction conditions and structural modifications that stabilize the ligated ribozyme preferentially accelerate ligation suggests that the transition state resembles ligated ribozyme more than it resembles the cleaved ribozyme−product complex.

A link between tertiary structure stability and the internal equilibrium between ligation and cleavage has been proposed to explain the difference between hammerhead and hairpin ribozymes in the propensity to catalyze ligation (*3*). Tertiary structure modifications also have been found to influence the internal equilibrium between cleavage and ligation reactions mediated by the hammerhead ribozyme. A structural constraint imposed by circularization of the substrate RNA was shown to shift the internal equilibrium in favor of cleavage by reducing the ligation rate constant (*36*) while a specific cross-linked form of the hammerhead ribozyme catalyzes cleavage and ligation with similar rate constants (T. K. Stage-Zimmerman and O. C. Uhlenbeck, personal communication). Thus, tertiary structure stability is a major determinant of ligation activity for both hammerhead and hairpin ribozymes.

The slow cleavage of S44 by R4 (Figure 2) reflects a change in the kinetic mechanism of reactions mediated by ribozymes that contain a four-way helical junction and not a defect in catalytic activity. Cleavage kinetics were simulated based on the kinetic mechanism shown in Figure 9 to test the notion that the apparent drop in cleavage rates results

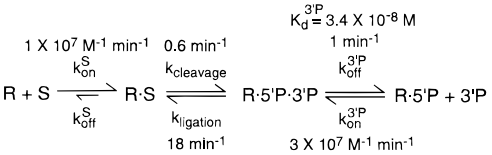

FIGURE 9: Kinetic mechanism of S44 cleavage by R4. The substrate binding rate constant is calculated from $k_{cleavage}/K_M^S$ values obtained from R4 cleavage reactions with S42 and S44. Substrate is assumed to bind irreversibly. Cleavage and ligation rate constants were obtained from LR43 self-cleavage and LR28 self-ligation rates, respectively. The 3′ product dissociation rate constant was calculated from $K_d^{3'P4}$, the cleavage and ligation rate constants, and the observed cleavage rate at saturating substrate concentrations. The 3′ product binding rate constant was calculated from $K_d^{3'P4}$ and the calculated 3′ product dissociation rate constant.

from rapid re-ligation of bound product. Over the same range of ribozyme concentrations that was used to determine kinetic parameters for cleavage of S44 by R4 (Figure 2B), an Eadie−Hofstee plot of simulated $k_{obs,cleavage}$ values gave $k_{cleavage,app} = 0.037$ min^{-1} and $K_M^S = 2.6$ nM, in good agreement with experimentally determined kinetic parameters. Thus, simulations support the conclusion that partitioning of bound product between dissociation and ligation leads to apparent inhibition of cleavage.

In the context of a four-way helical junction, tertiary contacts within and between helix−loop−helix domains contribute −3.7 kcal/mol to the product binding energy beyond that due to helical base pairs (Table 1). Despite the difference in size and complexity, hairpin and *Tetrahymena* ribozymes seem to share a similar mode of product binding. The P1 helix is the intermolecular helix that forms between the internal guide sequence of the *Tetrahymena* ribozyme and substrate or product RNAs. Like the two helix−loop−helix elements of the hairpin ribozyme, the P1 helix is in equilibrium between extended and docked states (*37*). Extrahelical interactions between the P1 helix and the *Tetrahymena* ribozyme core contribute ∼−6 kcal/mol to product binding energy (reviewed in *38*). Important contacts between the *Tetrahymena* ribozyme core and 2′-hydroxyls of both strands of the P1 helix have been identified from the loss in binding energy that results from specific deoxynucleotide substitutions (*39*−*42*). Specific deoxynucleotide substitutions in loop B and the ribozyme strand of loop A also have been found to impair hairpin ribozyme cleavage activity (*43*, *44*), leading to the proposal that a "ribose zipper" motif (*18*) mediates docking between loops A and B (*15*). Functional assays developed in the current study combined with time-resolved FRET measurements of docking equilibria provide a way to evaluate energetic contributions of specific functional groups to tertiary interactions within and between hairpin ribozyme structural elements.

The Arrhenius activation energy of 17 kcal/mol measured for self-cleavage of a hairpin ribozyme in the context of a four-way helical junction is similar to the Arrhenius activation energy previously measured for a minimal hairpin ribozyme (*25*). The temperature dependence of cleavage reactions catalyzed by a hairpin ribozyme with a four-way helical junction previously was reported to give a lower Arrhenius activation energy of 13.5 kcal/mol (*22*). This discrepancy might stem from differences in the specific hairpin ribozyme sequences used for the two studies. Alternatively, cleavage rate measurements in the previous study might have been complicated by a change in the kinetic mechanism if measured cleavage rate constants reflected ligation and product dissociation steps as well as the cleavage step. Despite a reduced activation barrier for ligation, $\Delta G^{\ddagger}$, we found individual $\Delta H^{\ddagger}$ and $\Delta S^{\ddagger}$ values for cleavage and ligation reactions to be the same, within experimental error, as those measured previously for minimal hairpin ribozymes (*25*). The similarity of thermodynamic parameters of cleavage and ligation reactions catalyzed by minimal hairpin ribozymes and ribozymes with a four-way helical junction provides no indication of any fundamental change in the nature of the rate-determining step or steps for reactions catalyzed by the two ribozyme structures.

ACKNOWLEDGMENT

I thank Steve Nesbitt for technical assistance, David Millar and Olke Uhlenbeck for sharing results before publication, and Dan Treiber, Jeff Orr, and Jamie Williamson for critical reading of the manuscript.

REFERENCES

1. Walter, N. G., and Burke, J. M. (1998) *Curr. Opin. Chem. Biol. 2*, 24−30.
2. Buzayan, J. M., Feldstein, P. A., Bruening, G., and Eckstein, F. (1988) *Biochem. Biophys. Res. Commun. 156*, 340−347.
3. Hertel, K. J., Herschlag, D., and Uhlenbeck, O. C. (1994) *Biochemistry 33*, 3374−3385.
4. Hertel, K. J., and Uhlenbeck, O. C. (1995) *Biochemistry 34*, 1744−1749.
5. Hegg, L. A., and Fedor, M. J. (1995) *Biochemistry 34*, 15813−15828.
6. Buzayan, J. M., Gerlach, W. L., and Bruening, G. (1986) *Nature 323*, 349−353.
7. Bruening, G., Passmore, B. K., van Tol, H., Buzayan, J. M., and Feldstein, P. A. (1991) *Mol. Plant−Microbe Interact. 4*, 219−225.
8. van Tol, H., Buzayan, J. M., and Bruening, G. (1991) *Virology 180*, 23−30.
9. Hampel, A., and Tritz, R. (1989) *Biochemistry 28*, 4929−4933.
10. Cai, Z., and Tinoco, I., Jr. (1996) *Biochemistry 35*, 6026−6036.
11. Butcher, S. E., Allain, F. H.-T., and Feigon, J. (1999) *Nat. Struct. Biol. 6*, 212−216.
12. Feldstein, P. A., and Bruening, G. (1993) *Nucleic Acids Res. 21*, 1991−1998.
13. Butcher, S. E., and Burke, J. M. (1994) *J. Mol. Biol. 244*, 52−63.
14. Komatsu, Y., Koizumi, M., Nakamura, H., and Ohtsuka, E. (1994) *J. Am. Chem. Soc. 116*, 3692−3696.
15. Earnshaw, D. J., Masquida, B., Müller, S., Sigurdsson, S. T., Eckstein, F., Westhof, E., and Gait, M. J. (1997) *J. Mol. Biol. 274*, 197−212.
16. Hampel, K. J., Walter, N. G., and Burke, J. M. (1998) *Biochemistry 37*, 14672−14682.
17. Pinard, R., Heckman, J. E., and Burke, J. M. (1999) *J. Mol. Biol. 287*, 239−251.
18. Cate, J. H., Gooding, A. R., Podell, E., Zhou, K., Golden, B. L., Kundrot, C. E., Cech, T. R., and Doudna, J. A. (1996) *Science 273*, 1678−1685.
19. Bassi, G. S., Murchie, A. I., Walter, F., Clegg, R. M., and Lilley, D. M. (1997) *EMBO J. 16*, 7481−7489.
20. Walter, N. G., Hampel, K. J., Brown, K. M., and Burke, J. M. (1998) *EMBO J. 17*, 2378−2391.
21. Murchie, A. I., Thomson, J. B., Walter, F., and Lilley, D. M. (1998) *Mol. Cell 1*, 873−881.
22. Thomson, J. B., and Lilley, D. M. J. (1999) *RNA 5*, 180−187.
23. Walter, N. G., Burke, J. M., and Millar, D. P. (1999) *Nat. Struct. Biol. 6*, 544−549.
24. Walter, F., Murchie, A. I. H., and Lilley, D. M. J. (1998) *Biochemistry 37*, 17629−17636.

25. Nesbitt, S. M., Erlacher, H. A., and Fedor, M. J. (1999) *J. Mol. Biol. 286*, 1009−1024.
26. Sambrook, J., Fritsch, E. F., and Maniatis, T. (1989) *Molecular cloning*: *A laboratory manual*, Cold Spring Harbor Laboratory Press, Cold Spring Harbor, NY.
27. Donahue, C. P., and Fedor, M. J. (1997) *RNA 3*, 961−973.
28. Nesbitt, S., Hegg, L. A., and Fedor, M. J. (1997) *Chem. Biol. 4*, 619−630.
29. Milligan, J. F., and Uhlenbeck, O. C. (1989) *Methods Enzymol. 180*, 51−62.
30. Burke, J. M., Butcher, S. E., and Sargueil, B. (1996) in *Catalytic RNA* (Eckstein, F., and Lilley, D. M. J., Eds.) pp 129−143, Springer-Verlag, Berlin.
31. Turner, D. H., Sugimoto, N., and Freier, S. M. (1988) *Annu. Rev. Biophys. Biomol. Struct. 17*, 167−192.
32. Fedor, M. J., and Uhlenbeck, O. C. (1990) *Proc. Natl. Acad. Sci. U.S.A. 87*, 1668−1672.
33. Uhlenbeck, O. C. (1995) *RNA 1*, 4−6.
34. Chowrira, B. M., Berzal-Herranz, A., and Burke, J. M. (1991) *Nature 354*, 320−322.
35. Esteban, J. A., Ranerjee, A. R., and Burke, J. M. (1997) *J. Biol. Chem. 272*, 13629−13639.
36. Stage-Zimmermann, T., and Uhlenbeck, O. (1998) *Biochemistry 37*, 9386−9393.
37. Bevilacqua, P. C., Kierzek, R., Johnson, K. A., and Turner, D. H. (1992) *Science 258*, 1355−1358.
38. Cech, T. R., and Herschlag, D. (1996) in *Catalytic RNA* (Eckstein, F., and Lilley, D. M. J., Eds.) pp 1−17, Springer-Verlag, Berlin.
39. Herschlag, D., Eckstein, F., and Cech, T. R. (1993) *Biochemistry 32*, 8299−8311.
40. Strobel, S. A., and Cech, T. R. (1993) *Biochemistry 32*, 13593−13604.
41. Pyle, A. M., Murphy, F. L., and Cech, T. R. (1992) *Nature 358*, 123−128.
42. Pyle, A. M., and Cech, T. R. (1991) *Nature 350*, 628−631.
43. Chowrira, B. H., Berzal-Herranz, A., Keller, C. F., and Burke, J. M. (1993) *J. Biol. Chem. 268*, 19458−19462.
44. Schmidt, S., Beigelman, L., Karpeisky, A., Usman, N., Sorensen, U. S., and Gait, M. J. (1996) *Nucleic Acids Res. 24*, 573−581.
45. Walter, F., Murchie, A. I. H., Thomson, J. B., and Lilley, D. M. J. (1998) *Biochemistry 37*, 14195−14203.

BI991069Q